



# Durability Evaluation of Clayey Sandy Soil Stabilized with Copper-Slag-Based Geopolymer Under Freezing–Thawing Cycles

Alireza Fakhrabadi<sup>1</sup> · Asskar Janalizadeh Choobbasti<sup>1</sup> · Saman Soleimani Kutanaei<sup>2</sup>

Received: 7 October 2021 / Revised: 28 March 2023 / Accepted: 19 May 2023  
© The Author(s), under exclusive licence to Chinese Society of Pavement Engineering 2023

## Abstract

In the current study, the durability of a clayey-sand stabilized with copper-slag (CS)-based geopolymer and alkaline activator solution (AAS) is investigated in freezing–thawing (F–T) cycles. For this purpose, tests including Atterberg limits, pH, standard Proctor compaction, unconfined compressive strength (UCS), accumulated loss of mass (ALM), swell and shrinkage, ultrasonic P-wave velocity, the toxicity characteristic leaching procedure (TCLP), and scanning electron microscopy (SEM) analysis were conducted. Various contents of CS (i.e., 0, 10%, and 15%) and 8 and 11 M NaOH were assessed in 0, 1, 3, 6, 9, and 12 cycles. The AAS contained 70% of  $\text{Na}_2\text{SiO}_3$  and 30% of NaOH. Also, the weight ratio of CS to ASS was 1 (CS/ASS = 1). According to the TCLP test, the CS-based geopolymer stabilized samples have no environmental hazards. The results illustrated that the strength and stiffness of untreated soil increased with an increase in F–T cycles until cycle 3. For samples with 11 M NaOH concentration, loss of strength and stiffness were observed due to F–T cycles. Furthermore, the sample with 8 M NaOH showed hybrid behavior (i.e., an increase in strength and stiffness until cycle 3), similar to that of untreated soil, and then declined until cycle 9, similar to soil treated with 11 M NaOH. Based on the microstructural analysis, higher microcracks were observed in the 8 M sample compared with the 11 M sample due to soft-strain behavior. Furthermore, a higher microcrack formation resulted in a higher potential for swell mass and volume change.

**Keywords** Durability · Freezing–thawing cycles · Copper slag · Geopolymer · Stabilization

## 1 Introduction

Every by-product material or traditional binder utilized for chemical stabilization has specific effects on the soil. Therefore, an extensive investigation of various soils is needed to recognize different aspects of binder effectiveness. The literature review indicates extensive research about geopolymer, but there are few investigations on the copper slag-based geopolymer and its durability against F–T cycles [1, 2]. On the other hand, the effects of CS-based geopolymer on the clayey sand are not considered yet. The chosen soil in the current paper is the combination of 20% clay with 80% Babolsar sand which can be utilized in geotechnical projects such as dam core, pavement, and Deep Soil Mixing

(DSM). This used soil has sufficient strength and permeability due to 20% of clay particles. The clay particles are smaller than sand particles; hence, clay particles can fill the pores between sand particles and enhance the strength and permeability of the whole soil fabric. The results and data of clayey-sand stabilized with CS-based geopolymer can be helpful in future geotechnical projects. Because of the possible workability of used soil in geotechnical projects, the durability of clayey sand stabilized with CS-based geopolymer must be investigated. The natural soil may be affected by snowy days during the year, so it is essential to evaluate the durability of clayey sand with F–T cyclic simulation.

For instance, in the western cities of Iran, such as Tabriz, soil and foundations may experience weathering conditions in cold regions. Thus, the geotechnical projects experience freezing and thawing (F–T) cycles at least once a year. These F–T cycles dramatically affect the durability and mechanical performances of soils and geotechnical structures like embankments and highway projects [3, 4]. Moreover, F–T cycles have positive effects on loose fine-grained soil, which leads to their stabilization

✉ Saman Soleimani Kutanaei  
samansoleimani16@yahoo.com

<sup>1</sup> Department of Civil Engineering, Babol Noshirvani University of Technology, 4714871167, Babol, Iran

<sup>2</sup> Department of Civil Engineering, Ayatollah Amoli Branch, Islamic Azad University, Amol, Iran

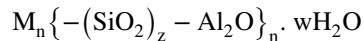
by increasing their compaction temporarily. Therefore, when these soils are used in wall, foundation, and tunnel construction because of freezing conditions, soil particle bonds become denser in disaggregated soils, especially in flocculated clay soil. As a result, deterioration of soil structure and ice segregation is induced due to negative pore water pressure [5, 6]. The degree of deterioration due to F–T cycles is described by some parameters such as freezing intensity, the number of cycles, type of cycles, duration of cycles, and the mechanical properties of geotechnical material used (e.g., void spaces, moisture content, capillarity, and type of soil, and the solubility of stabilization material) [3]. The prominent phenomenon that occurs during the F–T cycles is the formation of ice crystals in the air voids of the sample, which leads to the expansion of soil and creates microcracks. Afterward, the accessibility of melted ice to the microcracks is increased in the thawing stage, confirming the sample destruction [7].

On the other hand, lack of bearing capacity, swell or shrinkage, and soil settlement are significance concerns in many geotechnical projects. Also, with the increase in population growth and infrastructure demand, it is necessary to reclaim grounds for construction. Soil stabilization is a technique to improve soils' engineering and geotechnical properties such as mechanical strength, permeability, compressibility, durability, and plasticity [8, 9]. Most investigations have been based on a traditional binder, including Ordinary Portland Cement (OPC), fly ash, and lime. In addition to pollution, these materials produce a significant amount of CO<sub>2</sub> emissions, which contribute between 5 and 7 percent to global warming. The production of ordinary Portland cement, for instance, consumes a great deal of energy (5000 MJ), uses an extensive number of non-renewable resources (1.5 tons of limestone), and produces a great deal of carbon dioxide (1 ton CO<sub>2</sub> per ton of cement) [10–12]. In this regard, environmental-friendly additives have been utilized for soil improvement in chemical stabilization [13]. Recently, many researchers utilized binders like lime, Portland cement, and fly ash to produce geopolymer to stabilize the inappropriate soil [14–17].

Geopolymers, as mineral polymers obtained through geosynthesis, combine silico-aluminate sources with alkaline-activator solution [18–20]. Geopolymerization is the chemical reaction in which alumina (Al<sup>3+</sup> in IV-fold coordination) and silica from a silico-aluminate source (as a precursor) are dissolved by an alkaline-activator solution. These reactions create monomers and, finally, polycondensation of these monomers transforms solids to gel and produces Si–O–Al bonds [21, 22].

The Sialate network consisted of SiO<sub>4</sub> and AlO<sub>4</sub> tetrahedra linked alternately by sharing all the oxygens. For balancing the negative charges of Al<sup>3+</sup> in IV-fold coordination,

positive ions such as Na<sup>+</sup>, K<sup>+</sup>, Li<sup>+</sup>, Ca<sub>2</sub><sup>+</sup>, Ba<sub>2</sub><sup>+</sup>, NH<sub>4</sub><sup>+</sup>, and H<sub>3</sub>O<sup>+</sup> are required. Poly (Sialates) has the following empirical formula:



where “M” is a cation such as Na<sup>+</sup>, K<sup>+</sup>, and Ca<sub>2</sub><sup>+</sup>, “n” is the degree of polycondensation, “z” is the Si/Al molar ratio and may be equal to 1, 2, 3, or higher, and “w” is the water content.

Geopolymers exhibit higher mechanical and compressive strength, long-term durability, fast setting, low shrinkage, mitigate soil liquefaction, acid and fire resistance, and low CO<sub>2</sub> and other greenhouse gas emissions compared to OPC [11, 18, 19, 23–25].

Annually, about 24.6 million tons of slag is generated from the world copper production industry [26]. The disposal of waste materials like copper slag (CS) became a massive problem due to the lack of space for disposal. However, since these waste materials are used as a binder for soil improvement, they have caused lower pollution.

CS is an industrial by-product waste with a dark black color appearance. It contains a large amount of silica and alumina, which can be used as a precursor for the geopolymer base. CS is classified as poorly graded sand (SP), according to the USCS. The soil used in this study contains 20% of clay, which has SiO<sub>2</sub>, Ca, and Al<sub>2</sub>O<sub>3</sub>. However, because of a layered structure, strength development did not form, and thus higher amount of silica and alumina was required in the mixture for better geopolymerization. To deal with this issue, CS has been used [14, 26]. Alkaline-activator solution consists of alkali silicates, hydroxides, carbonates, or mixtures. In this regard, the combination of sodium hydroxide and sodium silicate has been widely used.

According to Liew et al. [18], alkali hydroxide is required to dissolve of aluminosilicate sources, while sodium silicate acts as a plasticizer. Because of its soluble silicate content, this silicate is preferred to other alkali activators. Also, due to the high amount of Si and Al atoms in this liquid, the geopolymerization rate enhanced. The parameters affecting the geopolymerization process include the raw material used as a base of geopolymer, the type and relative amount of alkali activator, and the curing condition (time and temperature). Therefore, both CS/L and Na<sub>2</sub>SiO<sub>3</sub>-to-NaOH ratios have remarkable effects on the workability of geopolymers. Heah et al. [27] investigated kaolin and alkali activator with S/L ratios. 6–1.2 and Na<sub>2</sub>SiO<sub>3</sub>/NaOH ratio of 0.16–0.36. The results showed that the compressive strength is affected by both S/L and Na<sub>2</sub>SiO<sub>3</sub>/NaOH ratios and increases with aging. The optimum S/L and Na<sub>2</sub>SiO<sub>3</sub>/NaOH ratios for this soil were 1 and 0.32, respectively. Also, the optimum molar ratios for Al<sub>2</sub>O<sub>3</sub>/Na<sub>2</sub>O and SiO<sub>2</sub>/Na<sub>2</sub>O were determined as 1.09 and 3.58, respectively.

Lu et al. [28] evaluated engineering properties such as volume, void ratio, collapsible settlement, and densely and loosely compacted loess microstructures against cyclic F–T. Their experimental results indicated that the dry densities decreased for the dense samples and increased for the loose samples with the increase in F–T cycles. Both void ratios tended to fall into a specific range. Hale and Shakoor [29] studied six sandstones to evaluate the effects of F–T cycles on their UCS values. The results showed that half of the sandstones lost their strength due to F–T cycles. Li et al. [30] investigated the correlation between mechanical behavior and the number of F–T cycles of compacted fine-grained soil using various tests, including F–T cycles, uniaxial compressive strength (UCS), unconsolidated-undrained triaxial compression test. According to their results, the F–T cycles affect the stress–strain plots and reduce the UC strength by 11%, elastic modulus by 32%, and cohesion by 84% after 31 F–T cycles, but the friction angle increased by 1–2°.

Tebaldi et al. [31] investigated clay stabilized with lime under the F–T cycles test and showed that with the increase in the number of cycles reduced the strength of samples. Solanki et al. and Bandara et al. [32, 33] studied three stabilization materials for subgrade soils, including hydrated lime, class C fly ash, and cement kiln dust, to examine the effects of F–T cycles on their UCS and resilient modulus. The results showed that UCS and  $M_r$  of stabilized soil with cementitious additives increased with the number of F–T cycles compared to raw soil specimens. However, all the specimens tested in the study showed a decrease in UCS values with an increase in the number of F–T cycles. Kamei et al. [3] investigated the effects of F–T cycles on UCS and the durability of soft clays stabilized with Bassanite. Based on the obtained results, the UCS and durability index decline with an increase in cycles.

In contrast, the increase in Bassanite content dramatically affected durability and strength improvement against F–T cycles. As a result, Bassanite can be considered appropriate material for stabilizing soft clay soils against F–T conditions. Liu et al. [4] studied the dynamic properties of cement- and lime-stabilized clay soils subjected to F–T cycles and indicated that clay soil endured F–T cycles with this stabilization. However, cement stabilized illustrated further strength and durability. Wu et al. [13] investigated the effects of F–T cycles on the expansive soil treated with steel slag powder (SSP) and cement. All tests were conducted at

a maximum of 12 F–T cycles with optimum moisture content. The study applied the samples to various curing times and temperatures (– 5 °C, – 10 °C, and – 15 °C). After each cycle, the volume change was measured, and UCS tests were performed. The results illustrated the increase in volume expansion due to temperature reduction. As the curing time increased, the effect of the F–T cycles on the volume change rate of the specimens reduced, and the UCS increased. The results have shown that the addition of SSP and cement improved the expansive soil; moreover, NaOH inhibited the degradation of the soil during an F–T cycle. Baldovino et al. [34] studied the mechanical properties of cement (3–9% by weight) treated silt which underwent various F–T cycles. Based on the results, the split tensile and unconfined compression strength was reduced due to an increase in F–T cycles; however, accumulated loss of mass (ALM) increased.

This study conducted laboratory tests to investigate the effect of CS-based geopolymer on enhancing the microstructural and mechanical properties of clayey-sand against F–T cycles. Its effects were evaluated by tests such as standard compaction, unconfined compressive strength, ultrasonic P-wave velocity, F–T cyclic test, swell, and shrinkage after specified cycles. Besides, scanning electron microscopy (SEM) analyses and pH tests were conducted to investigate the microstructural effects. According to recent studies on soil stabilized with non-environmentally-friendly binders, CS-based geopolymer has not been studied extensively regarding clayey-sand behavior against F–T cycles. For this purpose, all samples were subjected to 12 F–T cycles and then tested for the ultrasonic test, UCS test, height, and mass changes (Table 1).

## 2 Materials

### 2.1 Soil

A mixture of sand and 20% of clay was used in this study. The sand was obtained from the coast of Babolsar city in the north of Iran. According to the USCS system [35], this sand is poorly graded (SP). Figure 1 and illustrate the sand's grain size distribution and basic properties. The geotechnical characteristics of the sand are presented in Table 1. According to Table 2, the clay used in

**Table 1** Geotechnical properties of sand

Parameters	Description	Value	Standard method
$G_s$	Specific gravity	2.78	ASTM D854
$C_u = D_{60}/D_{10}$	Coefficient of uniformity	1.932	–
$C_c = [D_{30}^2/(D_{60} \times D_{10})]$	Coefficient of gradation	1.102	–
$D_{50}$	Mean grain size of the sand (mm)	0.214	–



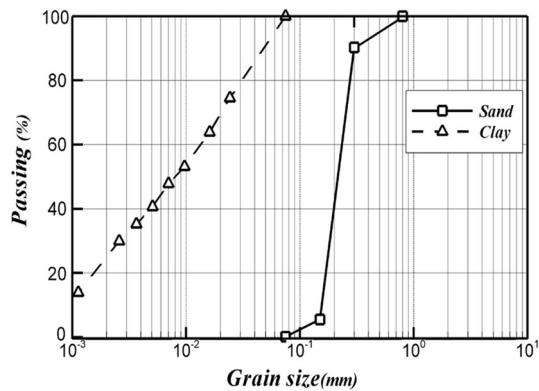


**Fig. 1** The grain size distribution of sand and clay

**Table 2** Atterberg limits of clay used in this study

Parameters	Description	Value	Standard method
$G_s$	Specific gravity	2.68	ASTM D854
LL	Liquid limit	52	ASTM D4318
PL	Plastic limit	20	ASTM D4318
PI	Plasticity index	32	ASTM D4318

this study was extracted from a trench near Amol city in Mazandaran province of Iran. This clay is a high-plasticity clay due to Atterberg limits. The SEM image of combined soil (sand + 20%clay) is shown in Fig. 2(a). As can be seen, the sample has a sharp and angular shape (sand) and planar particles (clay).

**Table 3** Chemical compositions of copper slag

Parameters	Weight (%)
Silica-SiO <sub>2</sub>	34
Alumina-Al <sub>2</sub> O <sub>3</sub>	2
Iron oxide-Fe <sub>2</sub> O <sub>3</sub>	47
Calcium oxide-CaO	6.5
Magnesium oxide-MgO	1.5

## 2.2 Copper Slag (CS)

CS is a by-product material obtained from matte smelting and refining of copper. At the end of copper production, two separate liquid phases form copper-rich matte (sulfides) and CS (oxides). When liquid slag cools slowly, it forms a dense, complex crystalline product, but if it cools quickly, it forms granulated amorphous slag [8]. The Pishro Company provided the CS used in this work in Kerman city. The SEM image of CS is illustrated in Fig. 2(b). The CS particles are angular with sharp edges. The composition and physical properties of CS chemicals are presented in Tables 3 and 4, respectively.

## 2.3 Alkaline-Activator Solution (AAS)

Using an alkaline-activator solution is essential for the geopolymerization process. Because of the low reaction pace between CS and water, another source of Si and Al is needed. Therefore, a combination of 30% of NaOH (for activation of Si and Al of copper-slag) with 70% of Na<sub>2</sub>SiO<sub>3</sub> (as a second resource of Si and Al) was used in

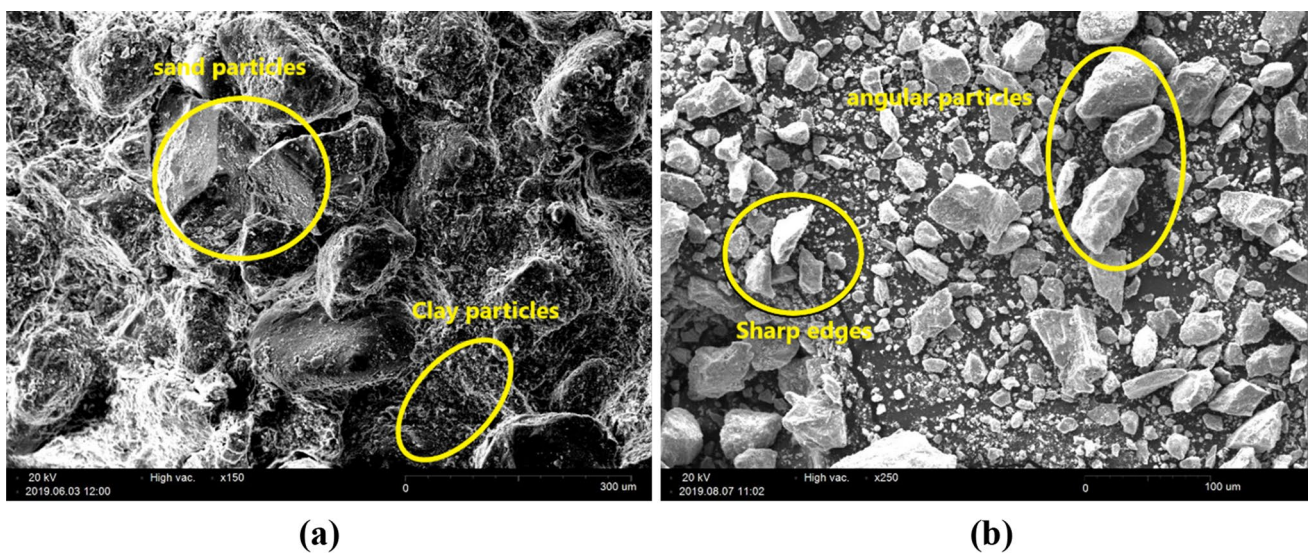


**Fig. 2** SEM images of: **a** soil: sand + 20% clay **b** Copper-slag

**Table 4** Physical properties of copper slag

Parameters	Analysis
Color	Black
Granule shape	Angular, sharp edges, multi-faceted
Hardness (Moh's scale)	7 Moh
Specific gravity	3.51
Bulk density	1.75 Tones/m
Conductivity	4 ms/s

this study. The NaOH pellets of 98% purity were provided in a 1 kg container from Ariashimi of Amol city. Also,  $\text{Na}_2\text{SiO}_3$  liquid with the  $\text{SiO}_2/\text{Na}_2\text{O}$  ratio of 2.48 was purchased from the Caspian Aftab Company of Amol city.

### 3 Sample Preparation

The samples were prepared using the under-compaction method (UCM) [36]. First, the sieved sand and clay were mixed for 5 min to achieve a uniform color. Next, the CS was added to the mixed soil. The required content of AAS with excess water (to provide the optimum moisture content) was mixed to obtain a homogeneous liquid based on the mentioned assumptions ( $\text{Na}_2\text{SiO}_3/\text{NaOH}$  and CS/L ratios). Eventually, all materials were mixed for 15 min and then placed in a mold with 50 mm diameter and 102 mm height in 5 layers. The total mass of mixed soil was divided into five portions and bagged in zipped packs separately. Each portion

was placed in one-fifth of the mold and compacted to reach the required level. For better interlocking of the layers, the surface of the first layer was scraped after the compaction. This process continued until the last layer [37, 38]. The compacted samples were cured for 14 days in a zipped plastic bag at ambient temperature ( $25 \pm 2$  °C) due to the effect of temperature on geopolymerization products. According to the literature, exceeding an optimum temperature and a long duration of heating may generate microcracks in samples and cause a moisture reduction [39–41].

## 4 Experimental Program

In this laboratory study, various tests, including eight Plasticity Index (PI), six standards Proctor compaction, 50 UCS before F–T condition, and 28 UCS after F–T condition, 13 SEM, 60 Ultrasonic P-Wave Velocity, 17 F–T cyclic test, and nine pH were performed. Table 5 demonstrates the combination of specimens, and Table 6 illustrates the UCS results for treated samples before F–T cycles.

### 4.1 Plasticity Index (PI) Test

According to ASTM D4318 [42], Atterberg limits were conducted on untreated soil and three chosen samples to investigate the PI changing after normal curing and F–T condition. PI indicates the strength, compressibility, permeability, swelling potential, and workability. Moreover, it indicates the amount of water that the sample remains in a plastic state [43].

**Table 5** Experimental program of treated soil

Sample name	CS (%)	NaOH concentration (M)	CS/ASS	$\text{Na}_2\text{SiO}_3/\text{NaOH}$	$\text{SiO}_2/\text{Na}_2\text{O}$
Soil15%CS-8 M	15	8	1	70/30	2.48
Soil10%CS-11 M	10	11	1	70/30	2.48
Soil115%CS-11 M	15	11	1	70/30	2.48

**Table 6** UCS tests of all mixtures in variation normal curing times

Curing	CS (%)	NaOH concentration (M)				
		2	4	8	11	15
2 days	10	48	48	90	143	225
	15	149	201	326	208	111
7 days	10	48	52	106	272	482
	15	143	226	548	726	529
14 days	10	23	37	92	265	503
	15	116	234	625	1097	1055
28 days	10	22	23	49	438	1000
	15	120	232	1250	1441	1355

## 4.2 pH Test

The pH can represent the development of reactions at the microstructural level and the strength of geopolymer-stabilized soil samples. After each F–T cycle, the pH test was conducted on the studied samples using a pH meter. pH tests were conducted according to ASTM D4972 [44]. At the end of the UCS tests, some parts of the samples were used for pH testing. The chosen portion of the sample was oven-dried at 40 °C to de-accelerate the geopolymerization process and then passed through sieve #10. Next, 40 gm of sieved soil was mixed with 40 gm of distilled water every 10 min for 1 h, and pH measurements were made [45, 46].

## 4.3 Compaction Test

According to ASTM D698 [47], the standard Proctor compaction test was conducted under three soil states. Soil without CS (untreated soil) and soil with 10% and 15% CS were used to evaluate the effect of CS on density. Soil with CS and alkaline-activator solution was defined as a CS-based geopolymer. Maximum dry density (MDD) and optimum moisture content (OMC) are necessary for sample preparation. Standard Proctor Compaction tests were conducted in two different series. The results of this test depend on the CS content and  $\text{Na}_2\text{SiO}_3/\text{NaOH}$  ratio. In the original series, two different CS contents were added to the soil to evaluate CS's effect on the soil's compaction characteristics. Another series of compaction, including soil with CS and alkaline-activator solution (AAS) (geopolymer), was also performed. Six standard Proctor compaction tests were conducted in the cylindrical mold with a diameter of 100.7 mm and a height of 117.2 mm to evaluate the effect of CS and geopolymer on soil separately. Dynamic compaction was conducted in three layers because a large portion of the soil was sand (granular particles) in this investigation. Hence, compacting it with a dynamic method instead of a static procedure is proposed.

## 4.4 Unconfined Compressive Strength Test (UCS)

Unconfined compressive stress is the maximum force applied per unit area during sample failure or the force applied until 15% of axial strain occurs. Various UCS tests were carried out to illustrate the impact of the stabilization of CS-Geopolymer on soil under F–T cycles following ASTM D2166 [48]. After 14 days of normal curing, samples were unwrapped and trimmed with the blade, and their diameter, height, and weight were determined. After 0, 1, 3, 6, 9, and 12 F–T cycles, the UCS test was performed at a constant displacement rate of 1% per minute.

## 4.5 F–T Cyclic Test

All the chosen samples were cured for 14 days, and then F–T cycling tests were applied according to ASTM D560 [49] after 0, 1, 3, 6, 9, and 12 cycles. The samples were put into the freezer at – 23 °C for 24 h (freezing stage) and then placed into an oven at 23 °C for another 24 h (thawing stage), making one F–T cycle (48 h.) After each cycle, UCS, mass loss, swell and shrinkage, pH, and P-wave velocity tests were conducted [3, 50, 51].

## 4.6 P-wave Velocity (Ultrasonic) Test

Ultrasonic waves are stress waves with frequencies higher than 20 Hz propagated in the mass matrix. These stress waves, referred to as longitudinal or primary waves are generated with two transducers called the “in-through” transmission test method. The frequency of the device was 54 Hz. In this method, one transducer was placed at the top surface of the sample, and the other was opposite the sample's surface. Then, the waves were introduced into the length of the samples. This instrument shows the time of wave propagation that travels the sample's length. Thus, P-wave velocity was obtained by dividing the sample length by wave travel time [52].

## 4.7 SEM Test

SEM is one of the tools widely used in nanotechnology. This technique provides pictures of samples for different investigations. In this method, the electron beam in a vacuum environment passes through the microscope vertically and then through the specimen's electromagnetic fields and special lenses. Immediately after colliding the beam with the sample, electrons and x-rays dissipate from the sample. Then, beams, electrons, and x-rays are gathered and presented as an SEM image. SEM images can help study morphology and composition of samples for microstructural investigations. Nine cubic specimens with a side length of 1 cm were cut, polished, and coated with gold to prevent the charging effects [53, 54].

# 5 Test Results and Discussions

## 5.1 Plasticity Index (PI)

PI results are provided in Table 7. The PI of samples was decreased with an increase in CS content due to cation exchange and chemical reactions between CS particles and AAS. PI is an indicator of clay content in the samples, and a decrease in PI value is accompanied by a reduction in the swell potential of clay particles [43].

**Table 7** Atterberg limits of mixtures before and after F–T cycles

Atterberg limits				
Sample name	LL before F–T	PL before F–T	PI before F–T	PI after F–T
Untreated soil	52	20	32	33
Soil15%CS-8 M	48	26	22	24
Soil10%CS-11 M	50	26	24	25
Soil15%CS-11 M	41	23	18	20

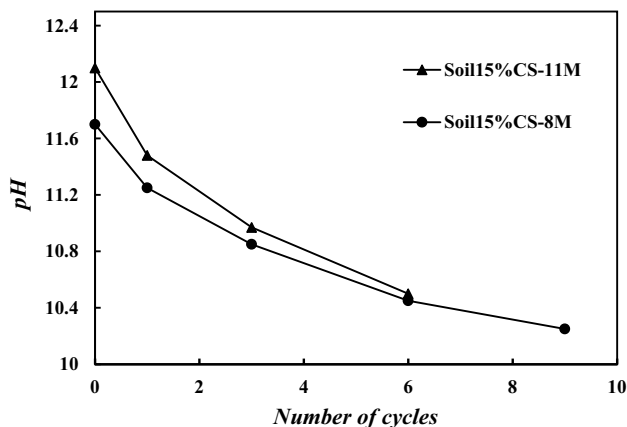
**Fig. 3** pH variation of stabilized soil after freezing–thawing cycles

Table 7 indicates a minor change in PI values for both treated and untreated soil samples after F–T cycles. Also, there was a reduction in PI before F–T cycles (i.e., normal curing condition). PI reduction of stabilized samples was observed due to chemical reactions between CS and clay particles, which causes the flocculation of clay particles and changes the soil matrix. This phenomenon leads to filling and coating the clay particles and, eventually, the decline of double-layer water thickness before F–T cycles. In the F–T conditions, the cause of the increase in PI is related to the degradation of the gel bond and the loss of geopolymerization, increasing the value of PI and therefore increasing the PI induced a higher water-holding capacity. These results are in agreement with those reported by other authors. For instance, Bin-Shafique et al. [55, 56] investigated the PI values before and after F–T cycles for two different clays with FA stabilization. The authors showed that, with an increase in FA content of unexposed samples, PI was decreased from 41 for 0% of FA to 18 for 10% of FA and 14 for 20% of FA. After F–T cycles, the PI values of stabilized soil with FA were increased by almost 13%, which is not statistically significant. This study observed an 8% increase in the PI values.

## 5.2 pH

It can be seen from Fig. 3 that the variation of pH concentration for two stabilized samples was decreased with

**Table 8** Compaction results of treated and untreated samples

Sample name	NaOH concentration (M)	Copper slag (%)	$\gamma_{d-max}$ (kN/m <sup>3</sup> )	$\omega$ (%)
Untreated soil	0	0	17.86	15.1
Soil10%CS	0	10	18.97	12
Soil15%CS	0	15	19.20	11.5
Soil15%CS-8 M	8	15	19.94	10.5
Soil10%CS-11 M	11	10	19.20	11.1
Soil15%CS-11 M	11	15	20.5	9.6

increasing the F–T cycles. The reduction in pH concentration is attributed to the dissolution of unreacted NaOH. With increasing the F–T cycles, OH<sup>-</sup> and Na<sup>+</sup> or Al<sup>+</sup> are consumed due to the geopolymerization process. However, under cyclic F–T conditions, pH reduction is related to the leaching of geopolymer bonds. With a higher NaOH concentration, higher pH values are achieved. “Soil15%CS-11 M” indicates the highest pH value regarding the lower mass loss [45, 57]. The pH value of “soil15%CS-11 M” decreased from 12.1 to 10.5 from cycles 0 to 6. Also, soil15%CS-8 M”, it decreased from 11.7 after cycle 0 to 10.2 after cycle 9 [58–63].

## 5.3 Standard Proctor Compaction

Table 8 presents the first series of compaction with CS. Adding the CS decreased the optimum moisture content (OMC) while the maximum dry density (MDD) increased. This behavior is related to two reasons:

- 1) CS has a smaller particle than sand and clay, which fills the pores. Eventually, it produces a mixture of higher density and consistency, increasing MDD [64, 65]. The particle size of CS affects OMC because these particles fill the voids and pores. Thus, the mixture has no space for water, and OMC decreases.
- 2) The specific gravity ( $G_s$ ) of CS is 3.51, suggesting a limited volume (compaction mold) and higher weight. As a result, an increase in MDD is reasonable.



The second series of compaction, which includes CS and AAS, are illustrated in Table 8. In all mixtures, adding AAS caused increasing the MDD and decreasing in OMC. Based on the obtained data, increasing CS content from 10 to 15% caused a 1% increase in MDD and a 4% decrease in OMC. Adding AAS, including 11 M NaOH, leads to a 6% increase in MDD and a 20% decrease in OMC. Adding 8 M NaOH causes a 4% increase in MDD and a 9.5% decrease in OMC. This behavior of AAS is attributed to PI differences between untreated soil and the soil stabilized with a geopolymer due to the presence of  $\text{Si}^+$  and  $\text{Al}^+$  in stabilized soil. As a result, it increases clay flocculation and consistency and reduces plasticity. Therefore, Atterberg limit tests were conducted on stabilized soil and found that soil improvement with geopolymer leads to a lower PI (18) for “soil15%CS-11 M” than untreated soil (32). Moreover, lower moisture absorption and OMC reduction were obtained. Hence, better compaction was observed due to lower volume changes [66].

#### 5.4 UCS and $E_{50}$

To evaluate the effect of F–T cycles on samples, the UCS tests were conducted on all samples after 0, 1, 3, 6, 9, and 12 cycles. Cycle 0 is 14 days of normal curing used for comparison with samples exposed to F–T cycles. The UCS tests were applied to the selected samples, including “soil15%CS-8 M”, “soil10%CS-11 M”, and “soil15%CS-11 M”. As part of this study, a comparison was made between unexposed stabilized samples (Cycle 0 = normal curing in 14 days) and the mentioned samples against F–T cycles (Cycles 1, 3, 6, 9, and 12) to illustrate how the mechanical behavior of the sample changes from cycle to cycle. The effect of the F–T cycles durability test depends on the soil type, classification, and properties of the stabilization material. Also, the solubility of stabilization material plays an essential role in the durability of samples [3].

The UCS test provided opposing results between stabilized and untreated soil samples. A different trend was observed from the information provided in the following figures. As shown in Fig. 4, for untreated soil, the strength of the samples was increased with an increase in the number of F–T cycles until cycle three and then continued with a minor change in the strength. Results showed that the soil exposed to a more significant number of F–T cycles became more brittle than the soil that had not been exposed to F–T cycles. This phenomenon can be attributed to variation in soil fabric in untreated soil exposed to the F–T cycle. When untreated soil is placed into the freezer cabinet, the pore water of the sample begins to freeze and turn into ice lenses. As a result, it produces ice pressure that affects soil structure and pushes soil particles together, leading to densification and aggregation of soil. Because of changing soil fabrics, untreated soil strength increases with an increase in F–T cycles until cycle

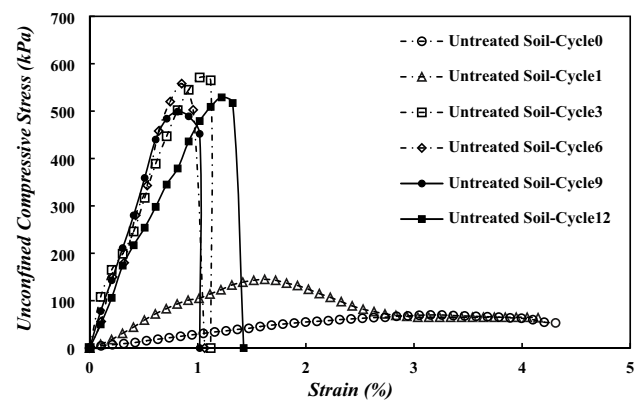


Fig. 4 Unconfined stress–strain relationship of untreated soil in various F–T cycles

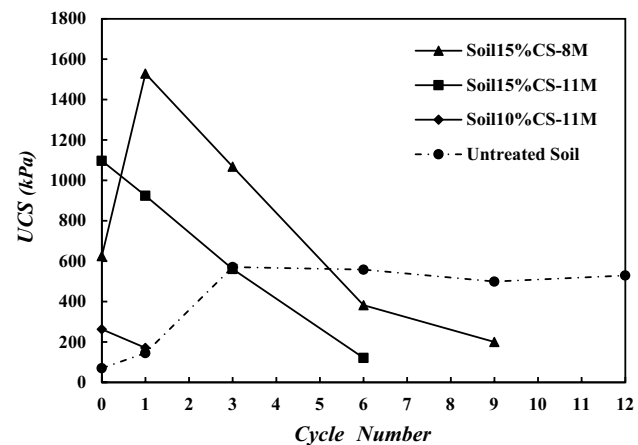


Fig. 5 The effect of F–T cycles on unconfined compression strength of treated and untreated samples

three. Afterward, a minor change occurred for further F–T cycles. This phenomenon may be related to balancing the ice pressure and resisting soil particles’ interlocking force. This result agrees with many other authors’ reports [28, 67–71].

It is evident from Figs. 5 and 6 that the UCS and  $E_{50}$  of the untreated sample have similar trends. Compared with untreated soil and chosen mixtures, complex results were observed with stabilized soil with CS-based geopolymer. All the selected mixtures failed to withstand twelve F–T cycles. “Soil15%CS-8 M”, “Soil15%CS-11 M”, and “Soil10%CS-11 M” endured nine cycles, six cycles, and one cycle, respectively. As a result of these contradictory results, it is also e to describe all mixtures comprehensively. A hybrid behavior was observed for the “soil15%CS-8 M” mixture. It is apparent from the data provided in Figs. 4, 5, 6, 7 that stress–strain, UCS, and  $E_{50}$  plots can separate into two sections; the first section includes cycles 0 to 3, and the second section contains



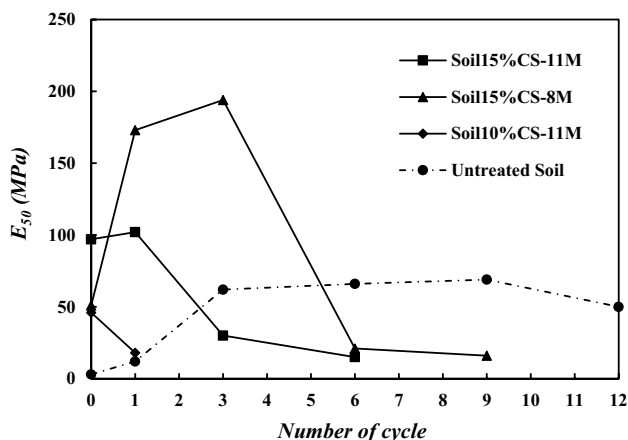


Fig. 6 E<sub>50</sub> variation under F–T cycles

cycles 3 to 9. It is evident from the first section of these plots (cycle 0–3) that “soil15%CS-8 M” has a similar trend to untreated soil. With an increase in F–T cycles, soil particles aggregated and compacted like untreated soil.

Meanwhile, after cycle 3, the strength and stiffness of the sample declined significantly, just like the two other mixtures. According to Table 6, this behavior is attributed to the geopolymerization process, which was not accomplished in 14 days of normal curing for “soil15%CS-8 M”. The difference in UCS values of “soil15%CS-8 M” between 14 and 28 days of normal curing was much higher than the UCS values difference in sample “soil15%CS-11 M”. Therefore, the geopolymerization process of “soil15%CS-8 M” was continued after the first few cycles [32, 72]. These results agree with the observations of Zhao et al. [73], who reported the effects of F–T cycles on red mud slurry-class F fly ash (RMSFAA). For 14-days-cured RMSFAA samples, further geopolymerization at the early stages of F–T conditioning was observed. Geopolymer stabilization in the current study differs from that of Lu et al. [28]. According to these authors, cement stabilization of expansive soil indicates a suitable response to F–T cycles despite the strength reduction. In other words, the cement-stabilized samples endured all 12 F–T cycles.

Conversely, from cycles 3 to 9, a dramatic reduction in strength and stiffness is observed due to the air voids within the samples. These air voids provide free space for the pore water content of the sample to change into ice crystals in the freezing stage. Moreover, the ice crystals create tensile stress that destroys particle interlocking and gel bonds (geopolymerization product). Therefore, the particles are disarranged, and microcracks are generated. In the thawing stage, melted ice penetrates microcracks and causes the dissolution of geopolymer gel. Eventually, gel reduction induces destruction in soil due to more accessibility of water in

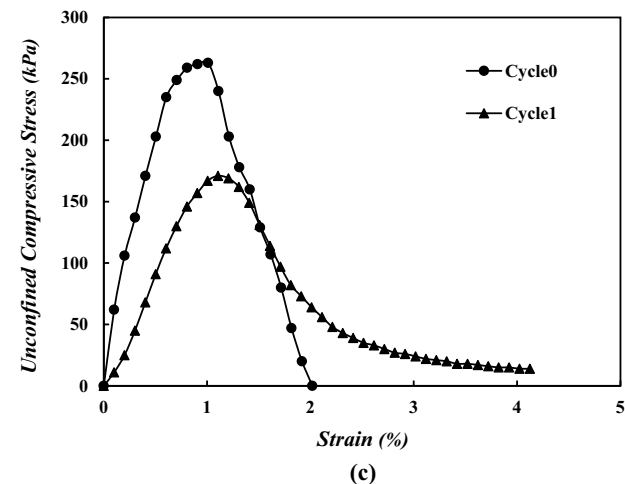
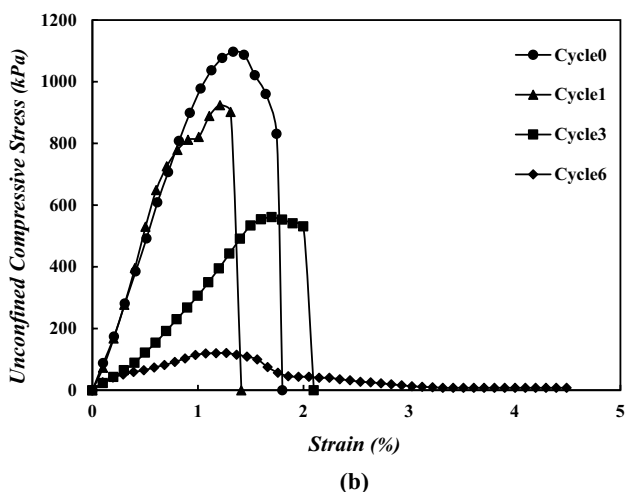
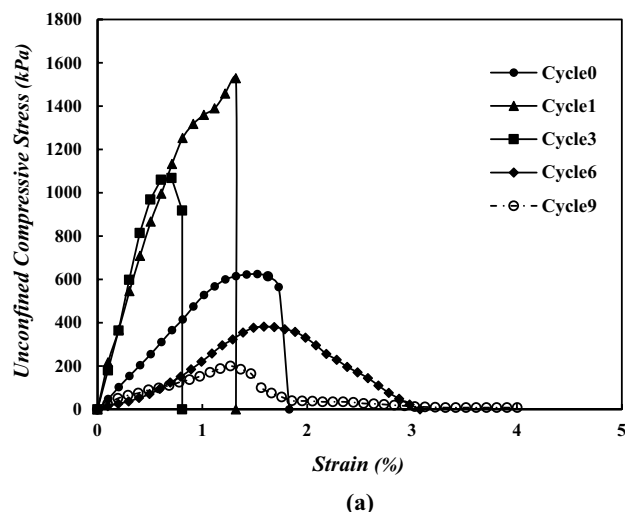


Fig. 7 Unconfined stress–strain relationship of: a “Soil15%CS-8 M” b “Soil15%CS-11 M” c “Soil10%CS-11 M” in various F–T cycles

microcracks, leading to a decrease in UCS [3, 32, 50, 72]. In “soil15%CS-11 M”, UCS decreased rapidly compared with “soil15%CS-8 M”. According to E<sub>50</sub> results in Fig. 6,

strain hardening of the sample changes to strain-softening after the first cycle.

The results show a remarkable decrease in the strength of “soil15%CS-8 M” and “soil15%CS-11 M”. The concentration and suitable content of alkaline-activator solutions are among the main parameters that play an essential role in activating CS. Activation of CS was guaranteed significantly in 14 days of normal curing for “soil15%CS-11 M” because of the high content of alkaline-activator concentration. Therefore, applying F–T cycles induced the formation of cracks and deterioration of gel bonds. Meanwhile, there was insufficient content of alkaline-activator solution to activate CS in “soil15%CS-8 M”. Thus, some portions of CS remained unreacted, which took time to be activated. Moreover, freezing of pore water provided suitable contact between AAS and CS. Eventually, most of them were activated, especially in the thawing stage. As more F–T cycles were applied, cracks and geopolymerization products were lost. Hence, the strength of samples declined with increasing the F–T cycles. According to Zhao et al. [73], strength increases for 14 days normal curing sample after five cycles were 50% while it was 15% for 28 days normal curing. This result agrees with that reported for “soil15%CS-8 M” UCS. The UCS of “soil15%CS-11 M” is more than “soil15%CS-8 M” at cycle 0. However, due to the F–T condition, a series of chemical reactions happened and caused an increase in “soil15%CS-8 M” strength compared to “soil15%CS-11 M”.

In F–T cycles, the flexibility of samples plays an essential role in the strength-changing rate of samples. “Soil15%CS-8 M” is more flexible than “Soil15%CS-11 M”. For instance, when ice pressure is applied to the soil structure of “soil15%CS-11 M”, the brittle structure of the sample prevents expansion. Thus, all the pressure is applied to geopolymeric links, leading to the deterioration of these bonds. The flexibility of “soil15%CS-8 M” caused a significant reduction in bond destruction and strength loss. Unlike untreated soil, soil with geopolymer stabilization indicates a strain-softening behavior with an increase in F–T cycles. Because the UCS test was applied after the thawing stage, the melted ice crystals existed in samples and reduced the brittle behavior of samples. As shown in Fig. 7(c), the most unstable sample is “soil10%CS-11 M”, which endured one cycle of the F–T cycling test. Nevertheless, the trend illustrates the reduction in strength and shifting from strain-hardening to strain-softening.

Figure 8 presents the pictures of the mixtures at various cycles. These pictures represent the procedure of deterioration of samples with the number of F–T cycles. As shown in Fig. 8(c), “soil10%CS-11 M” endured one cycle and collapsed after cycle two due to critical cracks experienced in the first cycle of F–T conditions. However, the rate of deterioration in soil with 8 M and 11 M was different. In “soil15%CS-8 M”, the shape of the sample was

stable until cycle 3, and just microcracks formed due to F–T cycles. After completion of CS activation, the destruction of the sample was begun, and critical cracks were formed in the sample due to the increasing number of cycles. Destruction appeared at the interface of layers, while in “soil15%CS-11 M,” the rate of destruction was faster. This destruction also appeared in the shape of the sample. Another reason for the deterioration of strength with increasing F–T cycles is the leaching of dissolved  $\text{Si}^+$  and  $\text{Al}^+$  by AAS at the thawing stage [45, 46].

Figure 6 presents the elastic modulus ( $E_{50}$ ), determined by the slope of a line connecting 50% of UC strength to the origin.  $E_{50}$  versus the number of F–T cycles indicates samples’ strain-hardening (brittle) and strain-softening (soft) behavior. As can be seen,  $E_{50}$  of untreated soil increased until cycle three and continued with minor change until cycle 12, which is in agreement with stress–strain plots. For stabilized soil, stiffness results indicate different trends; for instance, the  $E_{50}$  value of “soil15%CS-8 M” dramatically increased until cycle three and then declined sharply at cycle 9. This trend is related to the reasons mentioned above in the UCS section. From cycle 1 of F–T, the geopolymerization process and strength gaining started in the studied sample. Therefore, the soil fabric became denser, and the  $E_{50}$  value increased until the beginning of strength reduction. For “soil15%CS-11 M”, a minor change was observed after cycle one because of a slight change in UCS result due to completion of geopolymerization. Therefore, after cycle 1, the  $E_{50}$  value of “soil15%CS-11 M” decreased [74].

## 5.5 Absorbed Energy Results

Every stress–strain plot creates a specific area with the horizontal axis that illustrates the Absorbed Energy (AE), which means the energy required for the sample’s deformation. After a specified number of F–T cycles, AE was calculated from stress–strain plots and illustrated in Fig. 9. As can be seen, with an increase in the number of cycles, AE was decreased for both “soil15%CS-11 M” and “soil10%CS-11 M”. This reduction is related to the changing behavior of samples from hardening to softening. However, the AE of “soil15%CS-8 M” acted like untreated soil until cycle one and decreased until cycle 9. The higher AE shows that the tested specimen needs to apply higher stress to deform.

## 5.6 Mass Loss Results

According to Fig. 10, a dramatic contrast is observed between untreated soil and stabilized soil. The accumulated loss of mass is measured using Eq. (1).

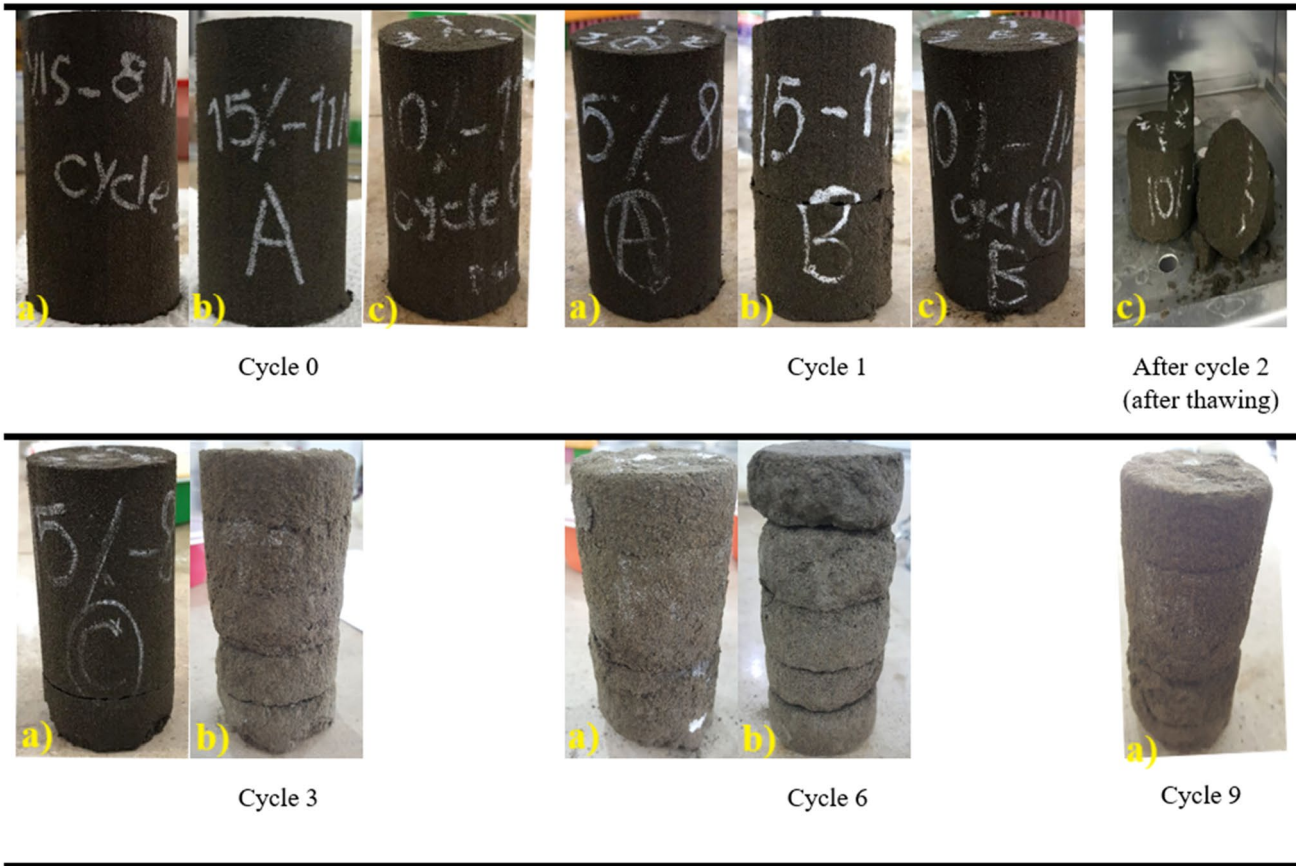


Fig. 8 Images of samples in variation F-T cycles; a soil15%CS-8 M b soil15%CS-11 M c soil10%CS-11 M

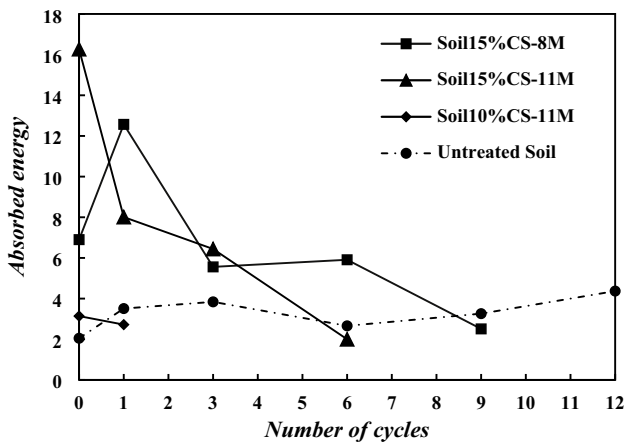


Fig. 9 Absorbed energy values versus number of cycles of all samples in various F-T cycles

$$ALM = \frac{m_{i,thaw} - m_{cycle0}}{m_{cycle0}} \times 100 \quad i = 1, 2, \dots, 12 \quad (1)$$

where ALM is the accumulative loss of mass (%),  $m_{i,thaw}$  is the mass of the sample after the first thawing cycle, and

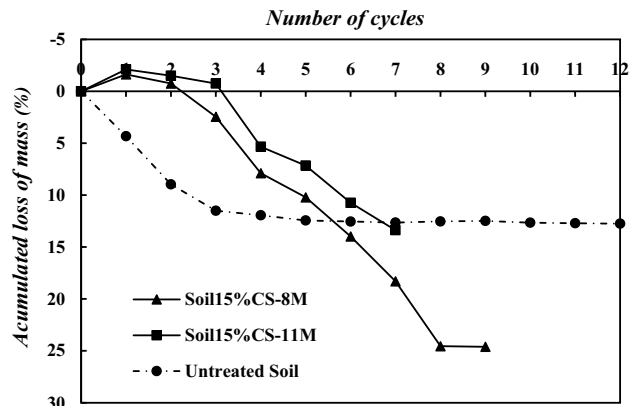


Fig. 10 Variation of accumulated loss of mass of samples due to F-T cycles

$m_{cycle0}$  is the mass of the unexposed sample after 14 days of normal curing.

According to Fig. 10, mass gain or loss is somehow related to absorbing or losing water due to F-T conditions. It is generally attributed to the extension of voids and dense states. Soil particles have a tight packing in dense samples.

Therefore, the interlocking force prevents the reduction of double-layer water, reducing water-absorbing potential. For stabilized soil, including “soil15%CS-8 M” and “soil15%CS-11 M,” gain of mass occurred until cycles 2 and 3, respectively. This phenomenon is related to freezing water content in samples in the freezing stage. Due to solid interlocking in earlier cycles, formed ice crystals cannot entirely be oven-melted at 23 °C. Hence, the mass of the sample was increased. With an increase in the number of cycles, the voids of the sample were filled with melted ice. In further cycles, there is no space for water in the freezing stage. Hence, the mass of samples gradually declined due to the ice crystals melting in the thawing stage. The flexibility of “soil15%CS-8 M” induced more swelling and shrinkage. Therefore, expansion and contraction sequences led to higher mass loss. Despite applying more load to soil particles and gel bonds, “soil15%CS-11 M” indicated a lower mass loss due to higher brittle behavior and lack flexibility [13, 75].

### 5.7 Swell-Shrinkage Results

Because of changes in diameter and height of the samples under F–T cycles, volume changes were calculated in this study to illustrate the swell (positive volume change) and shrinkage (negative volume change) of samples. Volume change of samples is obtained using Eq. (2), which indicates the total deformation after each cycle (after thawing):

$$\text{Volume Change} = \frac{V_{i,\text{thaw}} - V_{\text{cycle}0}}{V_{\text{cycle}0}} \times 100 \quad i = 1, 2, \dots, 12 \quad (2)$$

where  $V_{i,\text{thaw}}$  is the volume of samples after each cycle (after thawing) and  $V_{\text{cycle}0}$  is the volume of unexposed stabilized samples cured for 14 days under normal curing.

Figure 11 demonstrates a swelling behavior for untreated soil due to F–T cycles. The first reason for this result is the freezing of pore water in air voids, which causes expansion. The second reason is the higher content of swelling than shrinkage due to the cohesion of clay particles. In untreated soil, “forward migration” (i.e., water migration from the core of the sample to the surface) was higher than “converse migration” (i.e., water migration from the surface to the core of the sample). As a result, it leads to higher swelling of untreated soil. In contrast, however, stabilized soil showed a different behavior due to F–T cycles. They swelled until cycle three and then shrunk until they collapsed [76]. The higher the PI content, the higher the shrinkage potential was obtained. Therefore, with a concentration on the results provided in the PI section, it is evident that “soil15%CS-8 M” has a higher PI than “soil15%CS-11 M” after F–T cycles. Accordingly, it has more shrinkage potential than the soil with 11 M. According to mass loss results, a higher loss

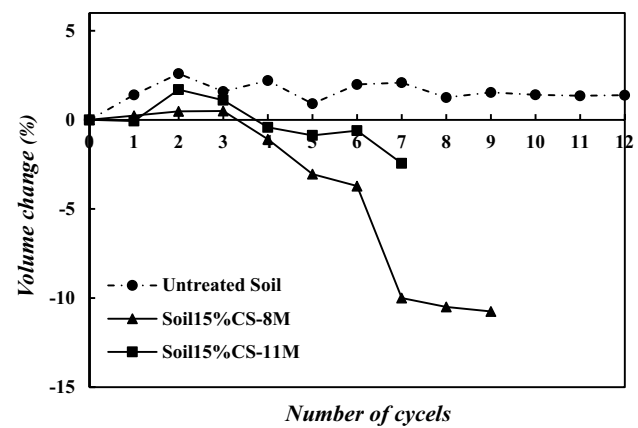


Fig. 11 Volume changes (swell and shrinkage) of the samples after each F–T cycles

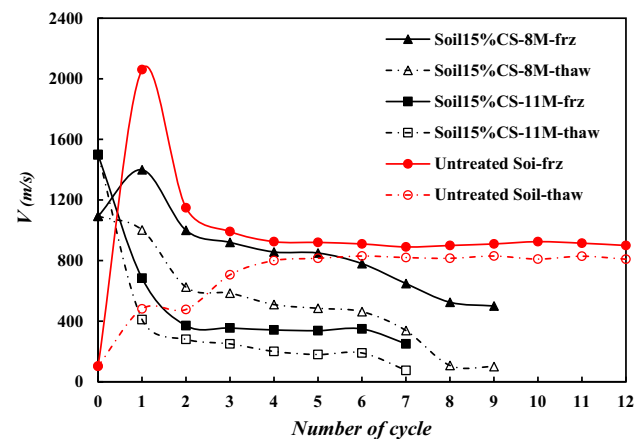


Fig. 12 P-wave velocity versus the number of cycles for both freezing and thawing condition

of gel bands was observed because of higher mass loss in “soil15%CS-8 M”, leading to more deformation [43].

### 5.8 P-wave Velocity Results

The P-wave velocity of all samples was calculated for each F–T cycle. In this regard, contradictory results were obtained for the untreated and stabilized sample. According to Fig. 12, with an increase in the number of cycles, the P-wave velocity of mixtures with 11 M NaOH was decreased in the same trends in freezing and thawing conditions, except for “soil15%CS-8 M” and untreated soil. From P-wave velocity plots of the untreated soil, it is evident that the trend of thawing and freezing conditions was different.

Two reasons contribute to changes in the P-wave velocity of the untreated sample: (1) the change in soil structure and (2) the water phase, which changed from liquid to ice lenses. For untreated soil in thaw condition,  $V_p$  was increased from



103 at cycle 0 to 809 m/s at cycle 12. This phenomenon is related to soil structure changing, which provides a compacted path for wave transmitting. Although the voids were increased due to structural change, it caused more closely connected particles in the solid soil matrix. Moreover, a dramatic drop was observed in the untreated soil after cycle 1 of the freezing stage. Figure 10 shows the mass loss of the sample, which is the reason for this phenomenon. Based on the mass content of the sample, it appears that the loss of pore water was related to the mass loss of F–T cycles.

Consequently, decreasing amounts of pore water cause fewer ice lenses to form, and thus fewer voids will be filled. In this way,  $V_p$  significantly decreased after the first cycle. The reason for the higher value of  $V_p$  in freeze conditions than in thawing conditions for stabilized soil is related to the freezing of pore water in the freezing stage. More voids were occupied due to the volume expansion of ice crystals. This phenomenon contributes to linking soil particles and thus densifying in the freezing stage. Eventually, P-waves travel in a shorter time in dense samples. In the thawing stage, melted ice was dissipated from the samples. As a result, the microcracks generated by the pressure of ice crystals were extended, particles' interlocking was destroyed, and the void ratio was increased. Thus P-waves must travel over longer distances due to these microcracks, and finally lower velocity is obtained [77–79].

## 5.9 TCLP Results

The TCLP test was conducted at 14 days of normal curing of CS-based geopolymer stabilized samples following USEPA method 1311 in Table 9. The investigated heavy metals were Arsenic (As), Bismuth (Bi), Cadmium (Cd), Chromium (Cr), Copper (Cu), Nickel (Ni), Lead (Pb), Selenium (Se), and Zinc (Zn). The results of TCLP tests are compared with the

**Table 9** TCLP results of CS-based geopolymer stabilized sample after 14 days of normal curing

Metal	Results of TCLP tests for soil15%CS-11 M sample on USEPA method 1311 (mg/L)	USEPA regulatory level (mg/L)
As	<0.63	5
Bi	BDL	N/R
Cd	<0.03	1
Cr	<0.05	5
Cu	<5.46	N/R
Ni	BDL	N/R
Pb	<0.75	5
Se	<0.38	1
Zn	<0.06	N/R

BDL Blow detectable limit, N/R Not regulated

Environmental Protection Agency's (EPA) regulated ranges in Table 9. Based on the TCLP analysis, the amounts of heavy metal in CS-based geopolymer stabilized samples are much lower than the EPA regulated ranges and have no environmental hazard [80, 81]

## 5.10 SEM Results

Figure 13 illustrates 11 SEM images for all mixtures in cycles 0, 1, 3, 6, and 9 to observe microstructural differences and similarities. Figure 13(a–e), (f–i), and (j–k) presents the effect of the number of F–T cycles on the microstructural and the rate of reactions of “soil15%CS-8 M”, “soil15%CS-11 M”, and “soil10%CS-11 M”, respectively. To better understand how microstructures developed, all mixtures were compared in each cycle. Previously, cycle 0 was defined as 14 days of normal curing that were not exposed to F–T cycles. As a result of data supplied by stress–strain and UCS plots, higher strength is inferred from “soil15%CS-11 M”, which is consistent with microstructural analysis. From Fig. 13(f), a dense gel structure with highly activated CS and few microcracks is observed, which justifies the higher value of UC strength of “soil15%CS-11 M”.

The microstructure of the samples dramatically changed during the F–T test. Figure 13(b) indicates the reactivation of unreacted CS. The strength was increased due to the geopolymerization and gel-forming process. Although more microcracks and some loose gel were formed, the strength of “soil15%CS-8 M” was higher than that of other samples. In “soil15%CS-11 M”, large destructive cracks are observed. These cracks lead to strength reduction of this sample compared with “soil15%CS-8 M”. In “soil10%CS-11 M”, destructive cracks and deterioration of gel bonds were formed enough to cause destruction and collapse of the sample at the end of the first cycle. Furthermore, a higher content of microcracks in “soil15%CS-8 M” than in “soil15%CS-11 M” caused a higher loss of mass and provided a higher potential for deformation. In other words, the higher the microcracks, the higher the potential for deformation (swell and shrinkage). With an increase in the number of destructive cracks, the value of UCS decreased. Reactions of CS in “soil15%CS-8 M” enhanced with a low rate of increase until cycle 3. According to Fig. 13(c), some dense gel formation and reactivation of remaining unreacted CS particles occurred due to the geopolymerization process. From cycle 3 to cycle 9, destructive and critical cracks were generated in “soil15%CS-8 M”, which led to strength deterioration. The SEM analysis indicates that an increase in the number of F–T cycles leads to two crucial facts: (1) the expansion of critical cracks and solution of geopolymerization products, which causes sample destructing, and (2) the reactivation of CS, which causes the generation of gel bonds and gaining strength [82].

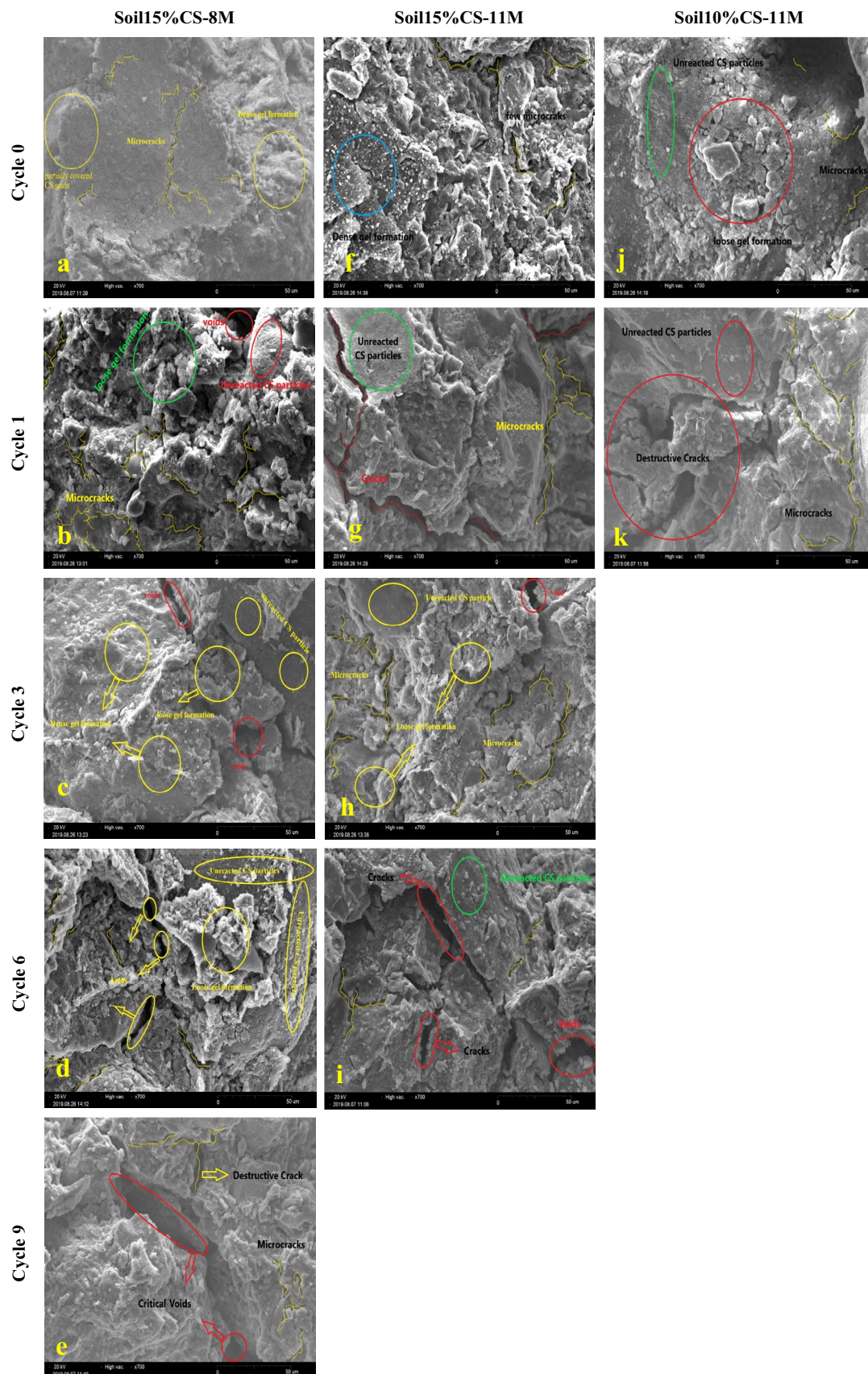


Fig. 13 SEM images of all mixtures in specified cycles

## 6 Conclusions

1. Before applying F–T cycles, the PI of stabilized soil was decreased. For instance, “soil15%CS-11 M” experienced a 44% reduction compared to the untreated soil, but after the F–T cycle, PI increased slightly. The pH values for stabilized soil decreased with an increase in the number of F–T cycles.
2. Due to the addition of CS and AAS to the soil, the MDD and OMC increased and decreased, respectively; i.e., adding 10% of CS resulted in a 6% increase in MDD and a 20% decrease in OMC.
3. The strength of clayey sand increases with increasing F–T cycles until cycle 3; after that, it shows minor changes. The UCS increased from 90 at cycle 0 to 590 kPa after cycle 12. Also, the behavior of the untreated sample changed from strain-softening to strain-hardening.
4. A 150% strength increase was observed for 8 M NaOH at cycle 1, and a 75% increase occurred in cycle 3. However, the strength declined to 33% and 67% for cycles 6 and 9, respectively. For “soil15%CS-11 M”, the UCS decreased to 91%, while “soil10%CS-11 M” collapsed after cycle 1.
5. The mass loss plot indicates that untreated soil mass loss increases to 13% by cycle three and continues with a minor change. In both stabilized soil samples, detrimental mass loss was obtained until cycle 3. Afterward, it declined to 14% for soil with 11 M and 25% for soil with 8 M. The swelling percentage of untreated soil was 2.5% approximately, and the shrinkage percentage for “soil15%CS-8 M” and “soil15%CS-11 M” was 10% and 2.5%, respectively.
6. In both freezing and thawing conditions,  $V_p$  decreased with an increase in cycle number. This reduction in freezing conditions was higher than the thawing condition. For instance, under freezing conditions, “soil15%CS-11 M” loses its velocity up to 80% in the last cycle.
7. According to SEM results, with an increase in cycle number, voids and microcracks increased due to the leaching of geopolymerization products. Moreover, it shows that the sample with 8 M NaOH has a higher potential to gain strength because of higher CS activation and geopolymerization.

## Declarations

**Conflict of Interest** The authors declare that they have no known competing financial interests or personal relationships that could have appeared to influence the work reported in this paper.

## References

1. Sahoo, S., & Singh, S. P. (2022). Strength and durability properties of expansive soil treated with geopolymer and conventional stabilizers. *Construction and Building Materials*, 328, 127078.
2. Miraki, H., Shariatmadari, N., Ghadir, P., Jahandari, S., Tao, Z., & Siddique, R. (2022). Clayey soil stabilization using alkali-activated volcanic ash and slag. *Journal of Rock Mechanics and Geotechnical Engineering*. <https://doi.org/10.1016/j.jrmge.2021.08.012>
3. Kamei, T., Ahmed, A., & Shibi, T. (2012). Effect of freeze-thaw cycles on durability and strength of very soft clay soil stabilised with recycled Bassanite. *Cold Regions Science and Technology*, 82, 124–129. <https://doi.org/10.1016/j.coldregions.2012.05.016>
4. Liu, X., Liu, J., Tian, Y., Chang, D., & Hu, T. (2019). Influence of the freeze-thaw effect on the Duncan-Chang model parameter for lean clay. *Transportation Geotechnics*, 21, 100273. <https://doi.org/10.1016/j.trgeo.2019.100273>
5. Chamberlain, E. J., & Gow, A. J. (1979). Effect of freezing and thawing on the permeability and structure of soils. *Developments in Geotechnical Engineering*, 26, 73–92.
6. Kravchenko, E., Liu, J., Krainiukov, A., & Chang, D. (2019). Dynamic behavior of clay modified with polypropylene fiber under freeze-thaw cycles. *Transportation Geotechnics*, 21, 100282. <https://doi.org/10.1016/j.trgeo.2019.100282>
7. Hotineanu, A., Bouasker, M., Aldaoud, A., & Al-Mukhtar, M. (2015). Effect of freeze-thaw cycling on the mechanical properties of lime-stabilized expansive clays. *Cold Regions Science and Technology*, 119, 151–157. <https://doi.org/10.1016/j.coldregions.2015.08.008>
8. Shi, C., Meyer, C., & Behnood, A. (2008). Utilization of copper slag in cement and concrete. *Resources, Conservation and Recycling*, 52, 1115–1120.
9. Kutanaei, S. S., Choobbasti, A. J., Fakhrabadi, A., Ghadakpour, M., Vafaei, A., & Afrakoti, M. P. (2022). Application of LRBF-DQ and CVBFEM methods for evaluating saturated sand liquefaction around buried pipeline. *Journal of Pipeline Systems Engineering and Practice*, 13, 4021077.
10. Mohammadinia, A., Arulrajah, A., Sanjayan, J., Disfani, M. M., Bo, M. W., & Darmawan, S. (2015). Stabilization of demolition materials for pavement base/subbase applications using fly ash and slag geopolymers. *Laboratory Investigation*. [https://doi.org/10.1061/\(ASCE\)MT.1943-5533.0001526](https://doi.org/10.1061/(ASCE)MT.1943-5533.0001526)
11. Kim, Y., Dang, M. Q., & Do, T. M. (2016). Studies on compressive strength of sand stabilized by alkali-activated ground bottom ash and cured at the ambient conditions. *International Journal of Geo-Engineering*. <https://doi.org/10.1186/s40703-016-0029-4>
12. Du, Y., Bo, Y., Jin, F., & Liu, C. (2015). Durability of reactive magnesia-activated slag-stabilized low plasticity clay subjected to drying–wetting cycle. *European Journal of Environmental and Civil Engineering*. <https://doi.org/10.1080/19648189.2015.1030088>
13. Wu, Y., Qiao, X., Yu, X., Yu, J., & Deng, Y. (2021). Study on properties of expansive soil improved by steel slag powder and cement under freeze-thaw cycles. *KSCE Journal of Civil Engineering*, 25, 417–428. <https://doi.org/10.1007/s12205-020-0341-6>
14. Yaghoubi, M., Arulrajah, A., Miri, M., Horpibulsuk, S., Darmawan, S., & Wang, J. (2018). Applied clay science impact of field conditions on the strength development of a geopolymer stabilized marine clay. *Applied Clay Science*. <https://doi.org/10.1016/j.clay.2018.10.005>
15. Phoo-ngernkham, T., Maegawa, A., Mishima, N., Hatanaka, S., & Chindaprasirt, P. (2015). Effects of sodium hydroxide



- and sodium silicate solutions on compressive and shear bond strengths of FA—GBFS geopolymer. *Construction and Building Materials*, 91, 1–8. <https://doi.org/10.1016/j.conbuildmat.2015.05.001>
16. Singhi, B., Islam, A., & Ali, L. M. (2016). Investigation on soil—geopolymer with slag, fly ash and their blending. *Arabian Journal for Science and Engineering*. <https://doi.org/10.1007/s13369-015-1677-y>
  17. Fakhrabadi, A., Ghadakpour, M., Choobbasti, A. J., & Kutanaei, S. S. (2021). Evaluating the durability, microstructure and mechanical properties of a clayey-sandy soil stabilized with copper slag-based geopolymer against wetting-drying cycles. *Bulletin of Engineering Geology and the Environment*, 80, 5031–5051.
  18. Liew, Y. M., Kamarudin, H., Al, A. M. M., Bnhussain, M., Luqman, M., Nizar, I. K., Ruzaidi, C. M., & Heah, C. Y. (2012). Optimization of solids-to-liquid and alkali activator ratios of calcined kaolin geopolymeric powder. *Construction and Building Materials*, 37, 440–451. <https://doi.org/10.1016/j.conbuildmat.2012.07.075>
  19. Davidovits, J., & Quentin, S. (1991). Geopolymers: inorganic polymeric new materials. *Journal of Thermal Analysis and Calorimetry*, 37, 1633–1656.
  20. Fakhrabadi, A., Ghadakpour, M., Choobbasti, A. J., & Kutanaei, S. S. (2021). Influence of the non-woven geotextile (NWG) on the engineering properties of clayey-sand treated with copper slag-based geopolymer. *Construction and Building Materials*, 306, 124830.
  21. Khale, D., & Chaudhary, A. R. (2007). Mechanism of geopolymerization and factors influencing its development: a review. *Journal of Materials Science*. <https://doi.org/10.1007/s10853-006-0401-4>
  22. Ghadakpour, M., Fakhrabadi, A., Janalizadeh Choobbasti, A., Soleimani Kutanaei, S., Vafaei, A., Taslimi Paein Afrakoti, M., & Eisazadeh, N. (2021). Effect of post-construction moisture condition on mechanical behaviour of fiber-reinforced-cemented-sand (FRCS). *Geomechanics and Geoengineering*. <https://doi.org/10.1080/17486025.2021.1980230>
  23. Zhang, M., Guo, H., El-korchi, T., Zhang, G., & Tao, M. (2013). Experimental feasibility study of geopolymer as the next-generation soil stabilizer. *Construction and Building Materials*, 47, 1468–1478. <https://doi.org/10.1016/j.conbuildmat.2013.06.017>
  24. Yaghoubi, M., Arulrajah, A., & Miri, M. (2018). Effects of industrial by-product based geopolymers on the strength development of a soft soil. *Soils and Foundations*. <https://doi.org/10.1016/j.sandf.2018.03.005>
  25. Behnood, A. (2018). Soil and clay stabilization with calcium- and non-calcium-based additives: a state-of-the-art review of challenges, approaches and techniques. *Transportation Geotechnics*. <https://doi.org/10.1016/j.trgeo.2018.08.002>
  26. Prasad, P. S., & Ramana, G. V. (2016). Feasibility study of copper slag as a structural fill in reinforced soil structures. *Geotextiles and Geomembranes*, 44, 623–640. <https://doi.org/10.1016/j.geotexmem.2016.03.007>
  27. Heah, C. Y., Kamarudin, H., Al, A. M. M., Bnhussain, M., Luqman, M., Nizar, I. K., Ruzaidi, C. M., & Liew, Y. M. (2012). Study on solids-to-liquid and alkaline activator ratios on kaolin-based geopolymers. *Construction and Building Materials*, 35, 912–922. <https://doi.org/10.1016/j.conbuildmat.2012.04.102>
  28. Lu, Y., Liu, S., Alonso, E., Wang, L., Xu, L., & Li, Z. (2019). Volume changes and mechanical degradation of a compacted expansive soil under freeze-thaw cycles. *Cold Regions Science and Technology*. <https://doi.org/10.1016/j.coldregions.2018.10.008>
  29. Hale, P. A., & Shakoob, A. (2003). A laboratory investigation of the effects of cyclic heating and cooling, wetting and drying, and freezing and thawing on the compressive strength of selected sandstones. *Environmental and Engineering Geoscience*, 9, 117–130. <https://doi.org/10.2113/9.2.117>
  30. Li, G., Ma, W., Wang, F., Mu, Y., Mao, Y., Hou, X., & Bing, H. (2015). Processes and mechanisms of multi-collapse of loess roads in seasonally frozen ground regions: a review. *Sciences in Cold and Arid Regions*, 7, 456–468.
  31. Tebaldi, G., Orazi, M., & Orazi, U. S. (2016). Effect of freeze-thaw cycles on mechanical behavior of lime-stabilized soil. *Journal of Materials in Civil Engineering*, 28, 72–81. [https://doi.org/10.1061/\(ASCE\)MT.1943-5533.0001509](https://doi.org/10.1061/(ASCE)MT.1943-5533.0001509)
  32. Solanki, P., Zaman, M., & Khalife, R. (2013). Effect of freeze-thaw cycles on performance of stabilized subgrade. *Geotechnical Special Publication*. <https://doi.org/10.1061/9780784412770.038>
  33. Bandara, N., Binoy, T.H., Aboujrad, H.S. (2015). Freeze–thaw durability of subgrades stabilized with recycled materials, proceeding international conference cold regions engineering 135–145. <https://doi.org/10.1061/9780784479315.013>
  34. de Jesús Arrieta Baldovino, J., dos Santos Izzo, R. L., & Rose, J. L. (2021). Effects of freeze–thaw cycles and porosity/cement index on durability, strength and capillary rise of a stabilized silty soil under optimal compaction conditions. *Geotechnical and Geological Engineering*, 39, 481–498. <https://doi.org/10.1007/s10706-020-01507-y>
  35. D2487. (2006). Standard practice for classification of soils for engineering purposes (unified soil classification system), ASTM Stand. Guid. D5521-05, 1–5. <https://doi.org/10.1520/D2487-11>
  36. Ladd, R. S. (1978). Preparing test specimens using undercompaction. *Geotechnical Testing Journal*, 1, 16–23.
  37. Ghadakpour, M., Choobbasti, A. J., & Kutanaei, S. S. (2020). Investigation of the Kenaf fiber hybrid length on the properties of the cement-treated sandy soil. *Transportation Geotechnics*. <https://doi.org/10.1016/j.trgeo.2019.100301>
  38. Choobbasti, A. J., & Kutanaei, S. S. (2017). Microstructure characteristics of cement-stabilized sandy soil using nanosilica. *Journal of Rock Mechanics and Geotechnical Engineering*, 9, 981–988.
  39. Horpibulsuk, S., Ph, D., Suksiripattanapong, C., Ph, D., Samingthong, W., Rachan, R., Ph, D., Arulrajah, A., & Ph, D. (2015). Durability against wetting—drying cycles of water treatment sludge—fly ash geopolymer and water treatment sludge—cement and silty clay—cement systems. *Journal of Materials in Civil Engineering*. [https://doi.org/10.1061/\(ASCE\)MT.1943-5533.0001351](https://doi.org/10.1061/(ASCE)MT.1943-5533.0001351)
  40. Shadnia, R., Zhang, L., Ph, D., & Asce, M. (2017). Experimental study of geopolymer synthesized with class F fly ash and low-calcium slag. *Journal of Materials in Civil Engineering*, 29, 1–10. [https://doi.org/10.1061/\(ASCE\)MT.1943-5533.0002065](https://doi.org/10.1061/(ASCE)MT.1943-5533.0002065)
  41. Leong, H. Y., Ek, D., Ong, L., Asce, M., Sanjayan, J. G., Nazari, A., & Ash, F. (2018). Strength development of soil—fly ash geopolymer: Assessment of soil, fly ash, alkali activators, and water materials. *Journal of Materials in Civil Engineering*. [https://doi.org/10.1061/\(ASCE\)MT.1943-5533.0002363](https://doi.org/10.1061/(ASCE)MT.1943-5533.0002363)
  42. D4318. (2014). Standard test methods for liquid limit, plastic limit, and plasticity index of soils 1. <https://doi.org/10.1520/D4318-10E01>
  43. Amadi, A. (2010). Evaluation of changes in index properties of lateritic soil stabilized with fly ash. *Leonardo Electronic Journal of Practices and Technologies*, 9, 69–78.
  44. D4972. (2013). Standard test method for pH of soils, ASTM Stand. Int. 1–4. <https://doi.org/10.1520/D4972-13.2>
  45. Aldaood, A., Bouasker, M., & Al-mukhtar, M. (2014). Impact of wetting—drying cycles on the microstructure and mechanical properties of lime-stabilized gypseous soils. *Engineering Geology*, 174, 11–21. <https://doi.org/10.1016/j.enggeo.2014.03.002>
  46. Cai, G., Liu, S., & Zheng, X. (2019). Influence of drying-wetting cycles on engineering properties of carbonated silt admixed



- with reactive MgO. *Construction and Building Materials*, 204, 84–93. <https://doi.org/10.1016/j.conbuildmat.2019.01.125>
47. D698. (2003). Standard test methods for laboratory compaction characteristics of soil using, 3
  48. D2166. (2013). Standard test method for unconfined compressive strength of cohesive soil 1, ASTM Int. i, 1–7. <https://doi.org/10.1520/D2166>
  49. D560-96. (2012). ASTM D560-96 standard test methods for freezing and thawing compacted soil-cement mixtures, i, 1–6. <https://doi.org/10.1520/D0560>
  50. Ahmed, A., & Ugai, K. (2011). Environmental effects on durability of soil stabilized with recycled gypsum. *Cold Regions Science and Technology*, 66, 84–92. <https://doi.org/10.1016/j.coldregions.2010.12.004>
  51. Roshan, K., Choobbasti, A. J., Kutanaei, S. S., & Fakhrabadi, A. (2021). The effect of adding polypropylene fibers on the freeze–thaw cycle durability of lignosulfonate stabilised clayey sand. *Cold Regions Science and Technology*, 193, 103418.
  52. Yesiller, N., Hanson, J. L., & Usmen, M. A. (2001). Ultrasonic assessment of stabilized soils. In *Soft Ground Technology*, pp. 170–181.
  53. Arrigoni, A., Pelosato, R., Dotelli, G., Beckett, C. T. S., & Ciancio, D. (2017). Weathering's beneficial effect on waste-stabilised rammed earth: A chemical and microstructural investigation. *Construction and Building Materials*, 140, 157–166. <https://doi.org/10.1016/j.conbuildmat.2017.02.009>
  54. Zhou, Z., Cai, X., Ma, D., Chen, L., Wang, S., & Tan, L. (2018). Dynamic tensile properties of sandstone subjected to wetting and drying cycles. *Construction and Building Materials*, 182, 215–232. <https://doi.org/10.1016/j.conbuildmat.2018.06.056>
  55. Bin-Shafique, S., Rahman, K., & Azfar, I. (2011). Geo-frontiers 2011 © ASCE 2011 697, Geo-Frontiers. 697–706
  56. Sharma, L. K., Sirdesai, N. N., Sharma, K. M., & Singh, T. N. (2018). Experimental study to examine the independent roles of lime and cement on the stabilization of a mountain soil: A comparative study. *Applied Clay Science*, 152, 183–195. <https://doi.org/10.1016/j.clay.2017.11.012>
  57. Saride, S., Puppala, A. J., & Chikyal, S. R. (2013). Swell-shrink and strength behaviors of lime and cement stabilized expansive organic clays. *Applied Clay Science*, 85, 39–45. <https://doi.org/10.1016/j.clay.2013.09.008>
  58. Ngo, T. P., Bui, Q. B., Phan, V. T. A., & Tran, H. B. (2022). Durability of geopolymer stabilised compacted earth exposed to wetting–drying cycles at different conditions of pH and salt. *Construction and Building Materials*, 329, 127168. <https://doi.org/10.1016/j.conbuildmat.2022.127168>
  59. Bian, X., Zeng, L., Ji, F., Xie, M., & Hong, Z. (2022). Plasticity role in strength behavior of cement-phosphogypsum stabilized soils. *Journal of Rock Mechanics and Geotechnical Engineering*, 14, 1977–1988. <https://doi.org/10.1016/j.jrmge.2022.01.003>
  60. Sukmak, P., De Silva, P., Horpibulsuk, S., & Chindaprasirt, P. (2015). Sulfate resistance of clay-Portland cement and clay high-calcium fly ash geopolymer. *Journal of Materials in Civil Engineering*, 27, 1–12. [https://doi.org/10.1061/\(asce\)mt.1943-5533.0001112](https://doi.org/10.1061/(asce)mt.1943-5533.0001112)
  61. Du, Y. J., Wu, J., Bo, Y. L., & Jiang, N. J. (2020). Effects of acid rain on physical, mechanical and chemical properties of GGBS–MgO-solidified/stabilized Pb-contaminated clayey soil. *Acta Geotechnica*, 15, 923–932. <https://doi.org/10.1007/s11440-019-00793-y>
  62. Salimi, M., & Ghorbani, A. (2020). Mechanical and compressibility characteristics of a soft clay stabilized by slag-based mixtures and geopolymers. *Applied Clay Science*. <https://doi.org/10.1016/j.clay.2019.105390>
  63. Wang, Y., Liu, X., Zhang, W., Li, Z., Zhang, Y., Li, Y., & Ren, Y. (2020). Effects of Si/Al ratio on the efflorescence and properties of fly ash based geopolymer. *Journal of Cleaner Production*, 244, 118852.
  64. Hoy, M., Ph, D., Horpibulsuk, S., Ph, D., Arulrajah, A., Ph, D., Mohajerani, A., & Ph, D. (2018). Strength and microstructural study of recycled asphalt pavement: Slag geopolymer as a pavement base material. *Journal of Materials in Civil Engineering*, 30, 1–11. [https://doi.org/10.1061/\(ASCE\)MT.1943-5533.0002393](https://doi.org/10.1061/(ASCE)MT.1943-5533.0002393)
  65. Lavanya, C., Rao, A. S., & Kumar, N. D. (2011). A review on utilization of copper slag in geotechnical applications, 14–17.
  66. Manjarrez, L., Zhang, L., & Asce, M. (2018). Utilization of copper mine tailings as road base construction material through geopolymerization. *Journal of Materials in Civil Engineering*, 30, 1–12. [https://doi.org/10.1061/\(ASCE\)MT.1943-5533.0002397](https://doi.org/10.1061/(ASCE)MT.1943-5533.0002397)
  67. Kaab, A. (2008). Remote sensing of permafrost-related problems and hazards. *Permafrost and Periglacial Processes*, 136, 107–136. <https://doi.org/10.1002/ppp>
  68. Othman, M. A., & Benson, C. H. (1993). Effect of freeze-thaw on the hydraulic conductivity and morphology of compacted clay. *Canadian Geotechnical Journal*, 30, 236–246. <https://doi.org/10.1139/t93-020>
  69. Tebaldi, G., Orazi, M., & Orazi, U. S. (2016). Effect of freeze-thaw cycles on mechanical behavior of lime-stabilized soil. *Journal of Materials in Civil Engineering*, 28, 1–6. [https://doi.org/10.1061/\(ASCE\)MT.1943-5533.0001509](https://doi.org/10.1061/(ASCE)MT.1943-5533.0001509)
  70. Viklander, P. (1998). Permeability and volume changes in till due to cyclic freeze/thaw. *Canadian Geotechnical Journal*, 35, 471–477. <https://doi.org/10.1139/t98-015>
  71. Ghazavi, M., & Roustaei, M. (2010). The influence of freeze-thaw cycles on the unconfined compressive strength of fiber-reinforced clay. *Cold Regions Science and Technology*, 61, 125–131. <https://doi.org/10.1016/j.coldregions.2009.12.005>
  72. Phasuphan, W., Praphairaksit, N., & Imyim, A. (2019). Removal of ibuprofen, diclofenac, and naproxen from water using chitosan-modified waste tire crumb rubber. *Journal of Molecular Liquids*. <https://doi.org/10.1016/j.molliq.2019.111554>
  73. Zhao, M., Zhang, G., Htet, K. W., Kwon, M., Liu, C., Xu, Y., & Tao, M. (2019). Freeze-thaw durability of red mud slurry-class F fly ash-based geopolymer: Effect of curing conditions. *Construction and Building Materials*, 215, 381–390. <https://doi.org/10.1016/j.conbuildmat.2019.04.235>
  74. Zhang, Y., Johnson, A. E., & White, D. J. (2019). Freeze-thaw performance of cement and fly ash stabilized loess. *Transportation Geotechnics*, 21, 100279. <https://doi.org/10.1016/j.trgeo.2019.100279>
  75. Ma, R., Jiang, Y., Liu, B., & Fan, H. (2021). Effects of pore structure characterized by synchrotron-based micro-computed tomography on aggregate stability of black soil under freeze-thaw cycles. *Soil and Tillage Research*, 207, 104855. <https://doi.org/10.1016/j.still.2020.104855>
  76. Yang, B., Ceylan, H., Gopalakrishnan, K., & Kim, S. (2017). Evaluation of the freeze and thaw durability of road soils stabilized with a biofuel co-product. *Geotechnical Special Publication*. <https://doi.org/10.1061/9780784480441.014>
  77. Yarbasi, N., Kalkan, E., & Akbulut, S. (2007). Modification of the geotechnical properties, as influenced by freeze-thaw, of granular soils with waste additives. *Cold Regions Science and Technology*, 48, 44–54. <https://doi.org/10.1016/j.coldregions.2006.09.009>
  78. Wang, D. Y., Zhu, Y. L., Ma, W., & Niu, Y. H. (2006). Application of ultrasonic technology for physical-mechanical properties of frozen soils. *Cold Regions Science and Technology*, 44, 12–19. <https://doi.org/10.1016/j.coldregions.2005.06.003>
  79. Eskişar, T., Altun, S., & Kalipcilar, I. (2015). Assessment of strength development and freeze-thaw performance of cement treated clays at different water contents. *Cold Regions Science and*

- Technology*, 111, 50–59. <https://doi.org/10.1016/j.coldregions.2014.12.008>
80. Xu, H., Gong, W., Syltebo, L., Izzo, K., Lutze, W., & Pegg, I. L. (2014). Effect of blast furnace slag grades on fly ash based geopolymer waste forms. *Fuel*, 133, 332–340. <https://doi.org/10.1016/j.fuel.2014.05.018>
  81. Tome, S., Etoh, M. A., Etame, J., & Sanjay, K. (2018). Characterization and leachability behaviour of geopolymer cement synthesised from municipal solid waste incinerator fly ash and volcanic ash blends. *Recycling*. <https://doi.org/10.3390/recycling3040050>
  82. Nazari, A., Bagheri, A., & Riahi, S. (2011). Properties of geopolymer with seeded fly ash and rice husk bark ash. *Materials Science and Engineering A*, 528, 7395–7401. <https://doi.org/10.1016/j.msea.2011.06.027>
- Alireza Fakhrebadi** successfully obtained his Master's degree from Babol Noshirvani University of Technology. He embarked on a Ph.D. journey at the University of Texas at Arlington in the United States. Currently, he serves as a Graduate Research Assistant, dedicating his efforts to advancing the field of geotechnical engineering and its practical applications.
- Asskar Janalizadeh Choobbasti** has doctoral of philosophy in Geotechnical Engineering. He is full professor and faculty of Geotechnical Engineering at the Department of Civil Engineering in Babol Noshirvani University of Technology.
- Saman Soleimani Kutanaei** has doctoral of philosophy in Geotechnical Engineering. He is assistant professor and faculty of Geotechnical Engineering at the Department of Civil Engineering in Ayatollah Amoli Branch, Islamic Azad University.

Springer Nature or its licensor (e.g. a society or other partner) holds exclusive rights to this article under a publishing agreement with the author(s) or other rightsholder(s); author self-archiving of the accepted manuscript version of this article is solely governed by the terms of such publishing agreement and applicable law.